Laser-enhanced fusion burn fractions for advanced fuels

John Jasper Bekx,[1] Siegfried Heinz Glenzer,[2] and Karl-Georg Schlesinger[3]
[1]*Ballaufstraße 9, 81735 Munich, Germany*
[2]*SLAC National Accelerator Laboratory, 2575 Sand Hill Road, Menlo Park, California 94025, USA*
[3]*BoS GmbH, St. Margarether Str. 7a, 7072 Mörbisch am See, Austria*

(Received 1 May 2024; accepted 6 August 2024; published 26 August 2024)

Calculations for the burn fraction in a laser-created plasma are presented, taking fuel depletion into account. The enhancement from a strong-field laser is analyzed and calculated in the Floquet-Volkoff framework, which was verified to provide an adequate theoretical prediction for laser-enhanced fusion cross sections in a previous work [Phys. Rev. C **109**, 044605 (2024)]. Three different fuels were considered for the fusion process, namely deuterium-tritium (DT) fusion, deuterium-helium fusion, and proton-boron fusion. Their laser-enhanced burn fractions are compared in idealistic and realistic settings, where both thermal and nonthermal distributions are considered. It is found that DT fusion gains the least relative enhancement to the burn fraction in all scenarios considered, and that the remaining fuels do not gain an absolute enhancement large enough to be appreciable in comparison with the former.

DOI: 10.1103/PhysRevC.110.024612

I. INTRODUCTION

Setting aside speculative statements regarding the origin and nature of dark energy, the universe's preferred method for energy production is, insofar as is known, nuclear fusion [1]. There has been a tenacious, decades-long pursuit of researchers to bring this sustainable, clean source of energy to a terrestrial scale. Despite steady progress [2–6] and impressive feats towards this goal have been achieved [7–11], a reliable reproducibility of this achievement appears to be far from trivial [12]. Moreover, the indirect drive ICF approach has so far been the only method to achieve this feat. After almost nine decades of research in the field of fusion, it may prove illuminating to gain insight from other fields that could aid in increasing fusion probabilities. One of these is the suggested enhancement due to the presence of a strong external laser field, which is slowly coming to its own as a field of research [13–24].

The justification behind the work done in this paper stems from three preceding works. In Bekx *et al.* [15], one of the main conclusions was that, though enormous enhancements to the fusion reaction arising from an external laser field can be highlighted when considering the fusion cross sections, it was not clear how much of these enhancements would persist in a realizable and observable setting. Thus, the consideration of a different theoretical diagnostic more closely related to observable quantities, such as the reactivity, is warranted. In Bekx *et al.* [22], we compiled four frequently used state-of-the-art theoretical models that attempt to predict the laser-induced enhancement to the nuclear fusion cross sections, and compared and discussed their respective differences—these methods being the Wentzel-Kramers-Brillouin (WKB) method, used in Refs. [13–15], the imaginary-time method (ITM), used in Ref. [15], the Kramers-Henneberger (KH) approach, employed in Refs. [16–20,22], and the Floquet-Volkoff (FV) method, as used in Refs. [14,21,22]. The semiclassical methods (WKB and ITM) were found not to generally hold for laser parameters of interest towards nuclear fusion enhancement. Finally, in Lindsey *et al.* [23], we compared the remaining analytical methods (KH and FV) with the results obtained from the numerical solutions of the time-dependent Schrödinger equation (TDSE) using a modified Crank-Nicolson (CN) scheme. The main result was the verification that the FV method managed to qualitatively follow the numerical cross-section results and even obtained quantitative results quite well, while largely discrediting the KH approach for modeling dynamic laser enhancement to nuclear fusion.

Following these conclusions, we provide in this work theoretical predictions for the laser-enhanced burn fractions of fusion fuels calculated with the FV method, in order to finally answer the question we posed in our first work [15], "whether current-day or near-future laser facilities will allow for observable [laser-induced] fusion enhancement."

II. THEORY

For the upcoming burn fractions, we will consider three different fusion fuels, namely deuterium-tritium fusion, deuterium-helium fusion, and proton-boron fusion:

$$ {}^{2}_{1}\mathrm{D} + {}^{3}_{1}\mathrm{T} \rightarrow {}^{4}_{2}\mathrm{He} + {}^{1}_{0}\mathrm{n} + 17.6\ \mathrm{MeV}, \tag{1} $$

$$ {}^{2}_{1}\mathrm{D} + {}^{3}_{2}\mathrm{He} \rightarrow {}^{4}_{2}\mathrm{He} + {}^{1}_{1}\mathrm{p} + 18.3\ \mathrm{MeV}, \tag{2} $$

$$ {}^{1}_{1}\mathrm{p} + {}^{11}_{5}\mathrm{B} \rightarrow 3\,{}^{4}_{2}\mathrm{He} + 8.7\ \mathrm{MeV}. \tag{3} $$

D and T refer to the isotopes ${}^{2}_{1}\mathrm{H}$ and ${}^{3}_{1}\mathrm{H}$, respectively. For each fusion reaction, the two colliding nuclei are described by an effective one-dimensional TDSE in terms of their relative

separation coordinate, $\mathbf{r}$, and their reduced mass, μ:

$$i\hbar\frac{\partial\psi(\mathbf{r},t)}{\partial t}=\left[-\frac{\hbar^2}{2\mu}\nabla_{\mathbf{r}}^2+V(r)+H_I(t)\right]\psi(\mathbf{r},t). \quad (4)$$

The relativistic rest mass energy, μc^2, for all considered fuel pairs is around 1 GeV, well above any energy scales considered in this work, justifying the use of such a nonrelativistic TDSE. The respective Coulomb repulsion is denoted by $V(r)=\kappa/r$, with $\kappa=e^2Z_1Z_2/4\pi\varepsilon_0$, and the interaction Hamiltonian, H_I, describing the interaction with the external laser field, is given in the velocity gauge and assumes the dipole approximation:

$$H_I=-\frac{eZ_{\text{eff}}}{\mu}\mathbf{p}\cdot\mathbf{A}(t)+\frac{e^2Z_{\text{eff}}^2}{2\mu}\mathbf{A}^2(t), \quad (5)$$

where $Z_{\text{eff}}=(Z_1A_2-Z_2A_1)/(A_1+A_2)$, Z_i and A_i denoting charge and mass numbers, respectively. The vector potential, $\mathbf{A}(t)$, is assumed to obey a harmonic time dependence $\mathbf{A}(t)=|\mathbf{A}|\sin(\omega t)$, defining the angular frequency ω, and is related to the electric field via $\mathbf{E}=-\partial\mathbf{A}/\partial t=-\omega|\mathbf{A}|\mathbf{e}_{\mathbf{A}}\cos(\omega t)$. The vector potential has no spatial dependence because of the imposed dipole approximation, which is valid so long as the wavelength of the laser field is much larger than the spatial extent of the fusing system, and was verified to be the case for all parameters considered in this work.

A. Floquet-Volkoff method

In the FV method, the effect of an external electric field to the fusion cross section is calculated as

$$\sigma(\mathcal{E},|\mathbf{E}|,\theta,\omega)=\sum_{n\in\mathbb{Z}}P_n(u,v)\sigma(\mathcal{E}+U_p+n\hbar\omega), \quad (6)$$

where $\mathcal{E}$ is the center-of-mass (CoM) energy of the two colliding nuclei, $|\mathbf{E}|$ is the electric-field strength, θ the polarization angle, and $\hbar\omega$ the photon energy. Furthermore, the ponderomotive energy is denoted by $U_p=(eZ_{\text{eff}}|\mathbf{E}|)^2/(4\mu\omega^2)$. The probability weight function is calculated as $P_n=|F_n(u,v)|^2$, with

$$F_n(u,v)=\frac{1}{2\pi}\int_0^{2\pi}d\xi\, e^{-iu\cos\xi+iv\sin 2\xi+in\xi}, \quad (7)$$

where u and v are dimensionless quantities given by $u=eZ_{\text{eff}}|\mathbf{E}|\sqrt{2\mu\mathcal{E}}\cos\theta/(\mu\hbar\omega^2)$ and $v=(eZ_{\text{eff}}|\mathbf{E}|)^2/(8\mu\hbar\omega^3)$. The cross section denoted on the right-hand side (RHS) of Eq. (6) is the field-free fusion cross section, calculated in the following parametrized form [25]:

$$\sigma(\mathcal{E})=\frac{S(\mathcal{E})}{\mathcal{E}}e^{-\sqrt{\frac{\mathcal{E}_G}{\mathcal{E}}}}, \quad (8)$$

with $\mathcal{E}_G=2\mu\kappa^2\pi^2/\hbar^2$ denoting the Gamow energy and $S(\mathcal{E})$ the astrophysical S factor. The latter was obtained from the work of Bosch and Hale [26] for DT and DHe^3 fusion, and provides a parametrized form for $S(\mathcal{E})$, which is valid for CoM energies in the ranges of [0.5, 550] keV and [0.3, 900] keV for DT and DHe^3, respectively. For pB^{11} fusion we employed the parametrization from Nevins and Swain [27]. For a full elaboration on the theoretical framework behind the FV method we refer to the works of Wang [21] and Liu *et al.* [14].

From the laser-enhanced cross section, we may calculate the laser-enhanced reactivity, assuming a thermalized Maxwellian velocity distribution, given by

$$\langle\sigma v\rangle=\sqrt{\frac{8}{\mu\pi(k_BT)^3}}\int_0^\infty d\mathcal{E}\,\sigma(\mathcal{E},|\mathbf{E}|,\theta,\omega)\,\mathcal{E}\,e^{-\frac{\mathcal{E}}{k_BT}}. \quad (9)$$

In the absence of an external laser, the integrand exhibits a peak at $\mathcal{E}_{\text{peak}}=(\mathcal{E}_Gk_B^2T^2/4)^{1/3}$ and the majority of contributions to the reactivity integral comes from CoM energies surrounding $\mathcal{E}_{\text{peak}}$, with a width of $\Delta=4\sqrt{\mathcal{E}_{\text{peak}}k_BT/3}$ [25]. It was verified that the integrand did not shift substantially outside of this range of CoM energies when considering the influence of the external field. Practically, the integrations were carried out up to an energy of $\mathcal{E}=200$ keV and were found to have converged for all temperatures considered in this work. Furthermore, all upcoming results refer to polarization averaged results, where

$$\sigma_{\text{ave}}(\mathcal{E},|\mathbf{E}|,\omega)=\frac{1}{2}\int_0^\pi d\theta\,\sin\theta\,\sigma(\mathcal{E},|\mathbf{E}|,\theta,\omega), \quad (10)$$

was used in Eq. (9) in place of $\sigma(\mathcal{E},|\mathbf{E}|,\theta,\omega)$.

B. Burn fractions

The burn fraction, $\Phi(t)$, is defined as the ratio between the total number of fusion reactions occurring at time t, $N_{\text{fus}}(t)$, and the total number of initial fuel pairs, $N_{\text{pair}}^{(0)}$:

$$\Phi(t)=N_{\text{fus}}(t)/N_{\text{pair}}^{(0)}. \quad (11)$$

If we consider an initial configuration of fuel of volume V_0 at a number density n_0, the initial number densities for each of the fuel components are

$$n_1^{(0)}=\alpha n_0=2\alpha N_{\text{pair}}^{(0)}/V_0 \quad (12)$$

$$n_2^{(0)}=(1-\alpha)n_0=2(1-\alpha)N_{\text{pair}}^{(0)}/V_0, \quad (13)$$

for some fuel mixture ratio $\alpha\in[0,1]$. Setting $\alpha=0.5$ refers to an equimolar mixture. Once fusion sets in, the number of fusion reactions, dN_{fus}, taking place over a time interval dt in the volume $V(t)$ is given by

$$dN_{\text{fus}}=\langle\sigma v\rangle(t)n_1(t)n_2(t)V(t)dt. \quad (14)$$

Integrating this equation provides us with $N_{\text{fus}}(t)$. However, the difficulty arises that every single term on the RHS of Eq. (14) is dependent on time and in an unknown way. The expansion of the laser plasma will cause $V(t)$ to increase up to a point where the resulting mixture density is too small to allow for fusion. The time within which fusion still occurs during this expansion is the confinement time, τ. Assuming, for example, a spherical pellet of fuel of radius R, the confinement time can be found to be $R/4c_s$ [25], where $c_s=\sqrt{4k_BT/(m_1+m_2)}$ is the isothermal sound velocity, and m_i denote ion masses. In addition, the fuel depletion will alter the velocity-distribution function and energies of the particles comprising the plasma. Hence, the reactivity $\langle\sigma v\rangle$ is also a time-dependent quantity.

To continue while allowing for a general volume geometry, let us make two simplifications:

(i) Assume the reactivity $\langle\sigma v\rangle$ remains a constant over the course of the confinement time τ.
(ii) Assume the volume remains a constant during the confinement time.

Note that this will lead to an overestimate of the burn fraction as we are only considering a decrease in fuel densities originating from fusion reactions, while neglecting the decrease from volume expansion. Additionally, no evolution of the temperature is considered, so during the confinement time, we only consider a constant value of $\langle\sigma v\rangle$ at a given temperature T. Note this implies we are neglecting the effect of the laser pulse on the ion velocity distribution. Whether making this assumption will lead to an overestimate of the fusion reactivity or not, we will address in Sec. III C. Making these assumptions is sufficient for the goal of this work, which is to examine the effect of laser-enhanced fusion on the burn fraction, rather than making highly accurate predictions thereof.

Defining $n_{\rm fus} = N_{\rm fus}/V_0$, Eq. (14) can be brought into the form

$$\frac{dn_{\rm fus}}{dt} = \langle\sigma v\rangle n_1 n_2. \tag{15}$$

Then, we know that the fuel densities are reduced through fusion reactions via:

$$n_1 = \frac{2\alpha N^{(0)}_{\rm pair}}{V_0} - n_{\rm fus} \tag{16}$$

$$n_2 = \frac{2(1-\alpha) N^{(0)}_{\rm pair}}{V_0} - n_{\rm fus}. \tag{17}$$

Using these relations in Eq. (15) and subsequently multiplying by $V_0/N^{(0)}_{\rm pair}$, we can obtain

$$\frac{d\Phi}{dt} = C(A-\Phi)(B-\Phi), \tag{18}$$

where we defined $A = 2\alpha$ and $B = 2(1-\alpha)$ and $C = N^{(0)}_{\rm pair}\langle\sigma v\rangle/V_0 = n_0\langle\sigma v\rangle/2$. This ordinary differential equation has an analytical solution:

$$\Phi(t) = \frac{Be^{A(Ct+c_0)} - Ae^{B(Ct+c_0)}}{e^{A(Ct+c_0)} - e^{B(Ct+c_0)}}. \tag{19}$$

The integration constant c_0 can be determined by requiring $\Phi(0) = 0$ and yields $c_0 = [\log(A/B) + 2\pi i\mathbb{Z}]/(A-B)$. As such, the burn ratio over the period of the confinement time τ is

$$\Phi(\tau) - \Phi(0) = \frac{AB[e^{AC\tau} - e^{BC\tau}]}{Ae^{AC\tau} - Be^{BC\tau}}. \tag{20}$$

This expression is consistent with the one for an equimolar mixture, where $A = B = 1$, and results in

$$\Phi(\tau) = \frac{C\tau}{1+C\tau} \tag{21}$$

$$= \frac{n_0\tau}{\frac{2}{\langle\sigma v\rangle} + n_0\tau}. \tag{22}$$

For a general fuel mixture α, the optimistic value of the burn ratio, which assumes a constant value of the reactivity over the confinement time, with a negligible effect on the densities from the expanding volume, is given by:

$$\Phi(\alpha,\tau) = 2\alpha(1-\alpha)\left[\frac{\eta^\alpha - \eta^{(1-\alpha)}}{\alpha\eta^\alpha - (1-\alpha)\eta^{(1-\alpha)}}\right], \tag{23}$$

where $\eta = \exp\{n_0\langle\sigma v\rangle\tau\}$. A generalization to a time-dependent reactivity and an expanding volume can be made by considering

$$\eta = \exp\left\{N^{(0)}_{\rm pair}\int_0^\tau dt\,\langle\sigma v\rangle(t)/V(t)\right\}, \tag{24}$$

but is not pursued here further, to refrain from fixing the geometry of the fusing plasma.

In what follows, we keep the volumetric geometry of the fusion plasma general, specifying everything in terms of the number density. The specific values that will be considered are $n_0 = 10^{23}\ {\rm cm}^{-3}$ and $n_0 = 7.25\times10^{26}\ {\rm cm}^{-3}$. The first value is chosen because it lies close to an average mass density of $\rho = n_0(m_1+m_2) = 1.0\ {\rm g\,cm}^{-3}$ for all three fuels, thus signifying a low-solid-density/liquid-density regime. It will be referred to as $n_{\rm low}$. The second value ($n_{\rm high}$) is the critical density for an electron plasma at the lowest photon energy that will be considered in the upcoming section ($\hbar\omega = 1$ keV). It signifies a regime of the number density above which it becomes increasingly improbable for the impinging laser to penetrate the fusing plasma, thus making the consideration of laser-induced enhancement obsolete for higher number-density regimes. We will neglect local fluctuations in the number density that an impinging laser pulse might induce. In addition, we keep the means for achieving sufficient fusion conditions unspecified as well. For this reason, we will treat the confinement time as a parameter that will provide insight into what values are necessary for an appreciable burn.

III. RESULTS

A. Peak burn-fraction estimates

Let us first consider a best-case-scenario estimate. For each of the fusion fuels DT, DHe^3, and pB^{11}, we assume $\langle\sigma v\rangle$ is simply given by its peak value. The integrand exhibits a peak at $\mathcal{E}_{\rm peak} = (\mathcal{E}_G k_B^2 T^2/4)^{1/3}$ and the majority of contributions to the reactivity integral comes from CoM energies surrounding $\mathcal{E}_{\rm peak}$. So, the peak value of the reactivity lies at that temperature for which $\mathcal{E}_{\rm peak}$ corresponds to the largest cross section. These values are obtained from Ref. [25] and are given in Table I, accompanied by the corresponding temperature and peak reactivity value. For these optimal plasmas exhibiting peak values of their respective reactivity, we can consider the equimolar burn fraction at the two aforementioned values for the number density from Eq. (22) as a function of the confinement time. This is shown in Fig. 1. The right-hand subplot of Fig. 1 is identical to the left-hand plot, but is shown on a log scale to better illustrate the subnanosecond behavior of the burn fraction. The value of $\Phi = 30\%$ is shown by the black dotted line, which signifies an appreciable burn-up fraction in inertial confinement fusion (ICF) [25,28].

We can observe from Fig. 1 that at both values of the number density the DHe^3 and pB^{11} fusion burn fractions are

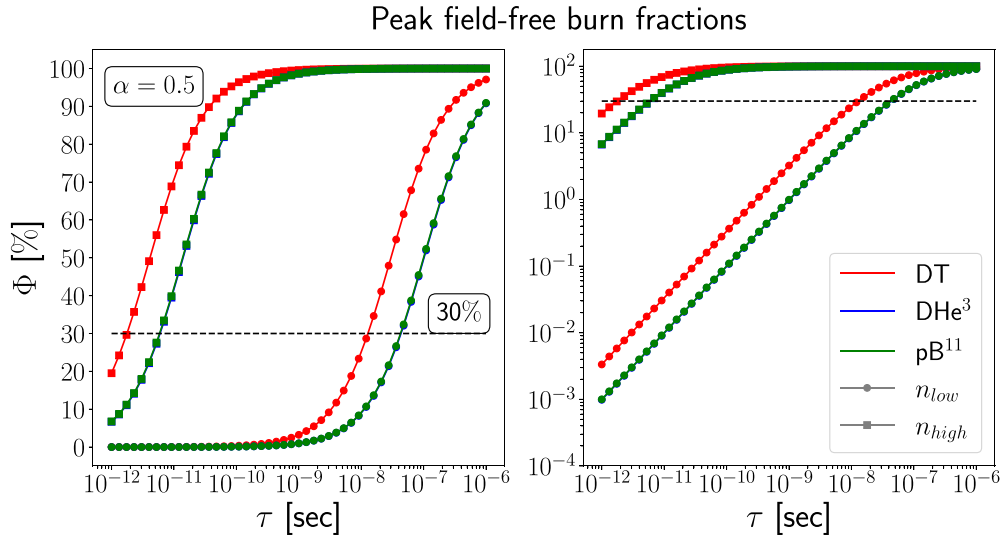

FIG. 1. (Left) The burn fraction Φ from Eq. (22) for an equimolar mixture of DT (red, $T = 29.8$ keV), DHe^3 (blue, $T = 115.0$ keV), and pB^{11} (green, $T = 171.5$ keV) at $n_{\text{low}} = 10^{23}$ cm^{-3} (circles) and $n_{\text{high}} = 7.25 \times 10^{26}$ cm^{-3} (squares) assuming the constant peak reactivities from Table I. The burn fraction of 30% is denoted by the black dotted line. (Right) Same figure, but plotted on a logscale to highlight the behavior at subnanosecond confinement times.

hardly distinguishable, which stems from the fact that the peak reactivities of both fuels are nearly the same. Recall however that the pB^{11} burn fraction is shown at the larger temperature of $T = 171.5$ keV as compared to the DHe^3 one at $T = 115.0$ keV. Furthermore, we can observe a drastic improvement in the burn fraction when considering the higher number density n_{high}, where appreciable burn up may be achieved on a picosecond confinement timescale. Conversely, for n_{low}, we require confinement times above 10 ns to get to burn fractions of the order of $\sim$1%.

For these same ideal-plasma parameters, we may investigate the effect of different fuel mixtures using Eq. (23), which is shown in Fig. 2. Figure 2 illustrates that the optimal value of the fuel mixture is $\alpha = 0.5$ to ensure the highest burn fraction for all fuels considered. Therefore, we will proceed by only considering equimolar fuel mixtures.

So far, we have just mimicked the conclusions of the well-known work of Lawson [29], namely that controlled fusion requires a combination of high plasma temperatures and high levels of compression. The purpose of this section was to address the method in aiding fusion by tailoring the energy distribution of the plasma particles so as to hit the peak of the reactivity. The temperature and density can be varied to achieve this. However, seeing as we wish to consider the effects of laser enhancement, the density can only be increased so much before the plasma becomes opaque to the laser, signified by n_{high} in this work. This leaves only the temperature as available parameter for reaching peak values of the reactivity, given by the ideal ones in this section. And though the resulting burn fractions are perhaps encouraging, the plasma temperatures corresponding to the peak reactivities considered so far do not coincide with realistic values. Typical temperatures in a laser-created plasma are of the order of a few keV. Thus, proceeding with the consideration of possible laser enhancement to the burn fraction, we will limit ourselves to temperatures within 1–10 keV.

TABLE I. Peak values for the reactivity of DT, DHe^3, and pB^{11}. The first column denotes the CoM value for which the cross section exhibits its maximum, which is in turn presented in the second column. The third column is the corresponding temperature for which the maximal value of the CoM energy corresponds to the peak value in the reactivity integral. The final column shows this maximal reactivity.

	$\mathcal{E}$ [keV]	σ [barn]	T [keV]	$\langle\sigma v\rangle$ [cm^3/s]
DT	64	5.0	29.8	6.68×10^{-16}
DHe^3	250	0.9	115.0	1.97×10^{-16}
pB^{11}	550	1.2	171.5	2.00×10^{-16}

B. Laser-enhanced burn fractions

In Fig. 3 we show the results for the laser-enhanced reactivity of DT, DHe^3, and pB^{11} as calculated by the FV method for electric-field strengths ranging from $|\mathbf{E}| = 10^{14}$–10^{17} V/m photon energies of 1, 5, and 10 keV. We can see that despite large cross-section enhancements that may arise at these parameters, illustrated in Ref. [22], the remaining effect on the reactivity may be quite limited, as seen in Figs. 3(a) and 3(b), thus substantiating the preliminary conclusions drawn in Ref. [15]. However, when considering $|\mathbf{E}| = 10^{17}$ V/m, we may observe that the reactivity for pB^{11} fusion at $\hbar\omega = 1$ keV manages to approach, and even surpass, the enhanced reactivity of DHe^3 fusion. For clarity, we draw attention to the large range of orders of magnitude depicted on the y axes in Fig. 3, which may obscure possible enhancements of below one order of magnitude.

With our laser-enhanced reactivity, we may now consider their implications surrounding the burn fractions. This is illustrated in Fig. 4. Because Fig. 3 illustrated that hardly any

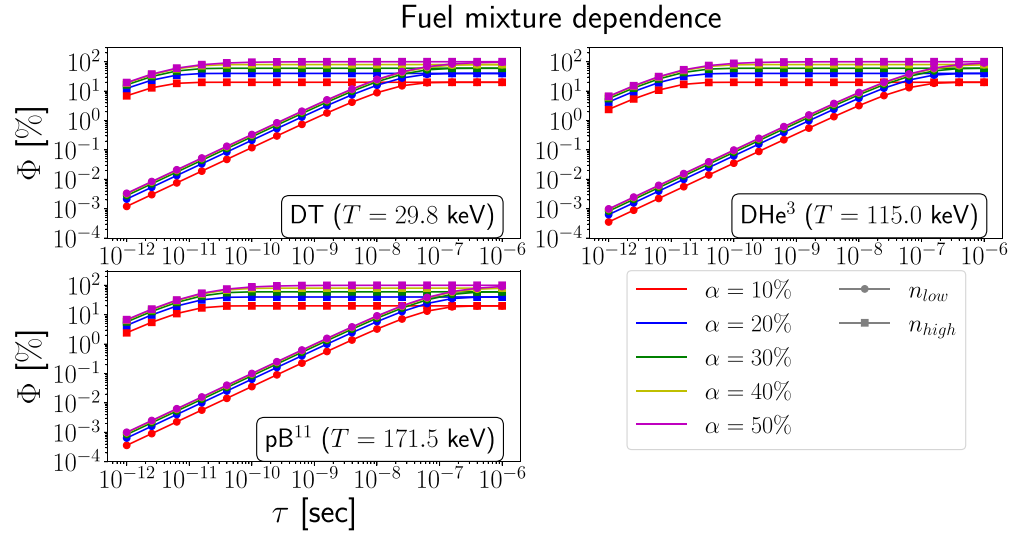

FIG. 2. The burn fraction Φ from Eq. (23) for varying fuel mixtures of DT (top left), DHe^3 (top right), and pB^{11} (bottom left) at $n_{\text{low}} = 10^{23}$ cm^{-3} (circles) and $n_{\text{high}} = 7.25 \times 10^{26}$ cm^{-3} (squares) assuming the constant peak reactivities from Table I.

laser enhancement to the reactivity is present for electric-field strengths below $|\mathbf{E}| = 10^{16}$ V/m, we only considered $|\mathbf{E}| = 10^{16}$ V/m and $|\mathbf{E}| = 10^{17}$ V/m for the subsequent burn fractions in Fig. 4, denoted in the left and right columns, respectively. The top and bottom rows illustrate the results for the number densities n_{low} and n_{high}, respectively. All results depicted in Fig. 4 are given at the single representative plasma temperature of $T = 3$ keV.

From the left two figures, we can see that even at $|\mathbf{E}| = 10^{16}$ V/m the laser enhancement to the burn fraction is below an order of magnitude for all photon energies and number densities considered. Only for pB^{11} can we see a deviation from the field-free burn-fraction line, denoted in black, which is a direct manifestation of the trend concluded in Ref. [22]. Namely that the relative laser-induced enhancement is largest for those fusing particles, which have the largest relative charge number.

However, this has an interesting consequence that can be seen in the right-side figures at $|\mathbf{E}| = 10^{17}$ V/m. For this value of $|\mathbf{E}|$ and at $\hbar\omega = 1$ keV, the burn fraction of pB^{11} manages to be nearly equal to the enhanced burn fraction of DHe^3. Nevertheless, we can see from Fig. 4 that even for the largest laser-induced enhancements, an appreciable burn (>1%) requires a confinement time beyond tens of nanoseconds, with DT as the one exception. For DT, appreciable burn can be obtained on the tens-of-picoseconds timescale,

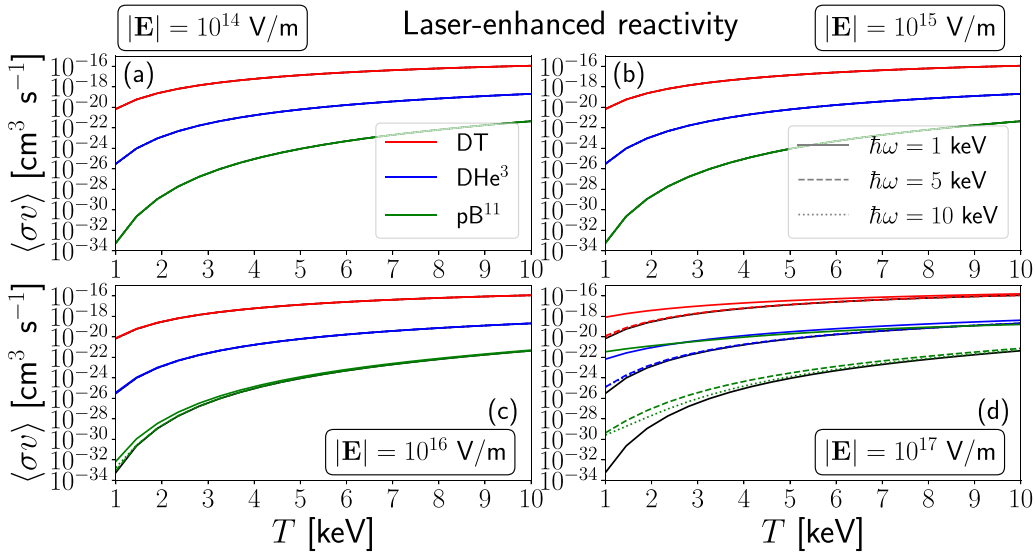

FIG. 3. The laser-enhanced polarization-averaged reactivity of DT (red), DHe^3 (blue), and pB^{11} (green) calculated with the FV method as a function of the temperature. The different subplots denote different electric-field strengths ranging from $|\mathbf{E}| = 10^{14}$–10^{17} V/m [(a)–(d)], whereas different photon energies are denoted by the solid ($\hbar\omega = 1$ keV), dashed ($\hbar\omega = 5$ keV), and dotted lines ($\hbar\omega = 10$ keV). The field-free reactivities for all fuels are denoted by the solid black lines.

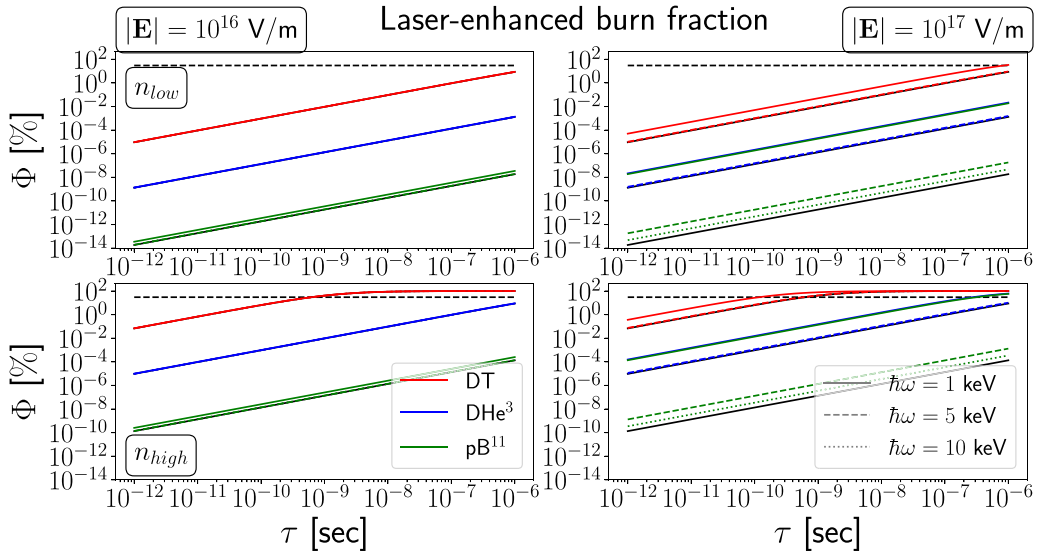

FIG. 4. The laser-enhanced burn fraction Φ from Eq. (22) for an equimolar mixture of DT (red), DHe^3 (blue), and pB^{11} (green) at $n_{\text{low}} = 10^{23}$ cm^{-3} (top row) and $n_{\text{high}} = 7.25 \times 10^{26}$ cm^{-3} (bottom row) using the reactivities as calculated with the FV method. The left and right columns refer to electric-field strengths $|\mathbf{E}| = 10^{16}$ V/m and $|\mathbf{E}| = 10^{17}$ V/m, respectively, whereas different photon energies are denoted by the solid ($\hbar\omega = 1$ keV), dashed ($\hbar\omega = 5$ keV), and dotted lines ($\hbar\omega = 10$ keV). The field-free reactivities for all fuels are denoted by the solid black lines and the black dotted line again denotes a burn fraction of 30%. The temperature considered is $T = 3$ keV.

but the laser enhancement is the smallest in this case. Nevertheless a maximal enhancement to the burn fraction of around one order of magnitude may still be observed for DT. Generally, we may note that if the external laser parameters induce an enhancement to the reactivity by a factor of f, then the burn fraction is increased by this same factor of f, so long as the product $n_0\tau$ is comparatively small [see Eq. (22)]. This is why we chose to show only one temperature $T = 3$ keV.

A final point we wish to analyze is whether or not the laser-induced enhancement to the fusion reactivity may be further aided by disembarking from the assumption of a thermalized plasma with a Maxwellian velocity distribution, which is briefly addressed in the following section. Similar considerations, moving away from a purely Maxwellian distribution, that study the effect of (a fraction of) the ion population lying at different energies indicate that this may indeed prove beneficial (see Refs. [30,31]).

C. Non-Maxwellian velocity distribution

For a thermalized Maxwellian distribution at a temperature T, the associated velocity distribution is given by:

$$f(\mathbf{v}) = Ae^{-\frac{\mu\mathbf{v}^2}{2k_BT}} = \left(\frac{\mu}{2\pi k_BT}\right)^{3/2} e^{-\frac{\mu\mathbf{v}^2}{2k_BT}}, \tag{25}$$

where the normalization constant, A, is obtained from normalizing $f(\mathbf{v})$ over all velocities $\mathbf{v}$ to 1. For considering non-Maxwellian velocity distributions, we do not wish to deviate too far from the Maxwellian one, on the grounds that a sensible analytic form for nonthermal velocity distribution is quite difficult to obtain. Moreover, a full dynamic nonthermal treatment is beyond the scope of this work. We merely wish to analyze to what extent even a small deviation from the fully thermalized framework would aid the burn fraction, in addition to the considered enhancement from the extreme electric field. To that end, we imagine the previous Maxwellian to exhibit an additional peak at some velocity $|\mathbf{v}_0|$, which can be larger or smaller than the location of the initial peak, at $\sqrt{2k_BT/\mu}$. This behavior can be expressed with

$$f(\mathbf{v}, \mathbf{v}_0) = A_1(1-\alpha)e^{-\frac{\mu\mathbf{v}^2}{2k_BT_1}} + A_2\alpha e^{-\frac{\mu(\mathbf{v}-\mathbf{v}_0)^2}{2k_BT_2}}, \tag{26}$$

where we allowed the second peak to differ in width as compared to the initial one, by introducing the second temperature T_2. Such a distribution could be realized naturally [31], or by, for instance, the injection of additional fusion fuel, in a plasma state, at a different average kinetic energy than the original mixture, characterized by the peak velocity $|\mathbf{v}_0|$. Of course, by simply adding fusion fuel, in conjunction with our inherent assumption that the fusing volume does not expand during the confinement time, would artificially raise the number density, thereby showing apparent enhancement that would be mistakenly attributed to the nonthermal nature of this fuel injection. Therefore, to remain consistent in our comparison with the thermalized results, we introduced the normalization constants A_1 and A_2. In order to have control over how much of the original mixture is reintroduced at the different velocity, we introduced the parameter α. It denotes the percentage by which the original Maxwellian population is reduced and added to the other population, such that we are consistently considering the same density. Subsequently, the terms in Eq. (26) are normalized to $(1-\alpha)$ and α, respectively. In doing so, we find that A_1 remains the same as with the original Maxwellian, i.e., $A_1 = (\mu/2\pi k_BT_1)^{3/2}$. For

the second term, we use

$$\begin{aligned} 1 &= \int d^3\mathbf{v} A_2 e^{-\frac{\mu(\mathbf{v}-\mathbf{v}_0)^2}{2k_BT_2}} \\ &= 2\pi A_2 \int_0^\infty dv v^2 e^{-\frac{\mu(v^2+v_0^2)}{2k_BT_2}} \int_{-1}^{1} d\cos\theta e^{\frac{\mu v v_0 \cos\theta}{k_BT_2}} \\ &= 2\pi A_2 \frac{k_BT_2}{\mu v_0} \int_0^\infty dv v \left[e^{-\frac{\mu(v-v_0)^2}{2k_BT_2}} - e^{-\frac{\mu(v+v_0)^2}{2k_BT_2}} \right]. \end{aligned} \tag{27}$$

The relevant integrals can be converted to a Gaussian-like ones:

$$\begin{aligned} \int_0^\infty dv v e^{-\frac{\mu(v\pm v_0)^2}{2k_BT_2}} &= \frac{k_BT_2}{\mu} e^{-\frac{\mu v_0^2}{2k_BT_2}} \\ &\quad \mp \frac{v_0}{2}\sqrt{\frac{2\pi k_BT_2}{\mu}} \operatorname{erfc}\left(\pm \sqrt{\frac{\mu v_0^2}{2k_BT_2}} \right). \end{aligned} \tag{28}$$

Thus, the integral in Eq. (27) results in $\sqrt{2\pi v_0^2 k_BT_2/\mu}$, and subsequently $A_2 = (\mu/2\pi k_BT_2)^{3/2}$. An unsurprising result, given that the second term in Eq. (26) is a shifted Gaussian distribution.

It is illustrative to see how this new distribution behaves as a function of $\mathcal{E}$. From $f(\mathcal{E})d\mathcal{E} = f(\mathbf{v})d^3\mathbf{v}$ and using $\mathcal{E} = \mu v^2/2$, we may obtain

$$\begin{aligned} f(\mathcal{E}, \mathcal{E}_0) = 2(1-\alpha)\sqrt{\frac{\mathcal{E}}{\pi (k_BT_1)^3}} e^{-\frac{\mathcal{E}}{k_BT_1}} \\ + \frac{\alpha}{\sqrt{\pi k_BT_2 \mathcal{E}_0}} \sinh\left[\frac{2\sqrt{\mathcal{E}\mathcal{E}_0}}{k_BT_2} \right] e^{-\frac{(\mathcal{E}+\mathcal{E}_0)}{k_BT_2}}, \end{aligned} \tag{29}$$

where $\mathcal{E}_0 = \mu v_0^2/2$ was introduced. For the remainder of this section, we will assume $T_1 = T_2 \equiv T$, i.e., we do not allow the fuel fraction that was reintroduced at the different peak velocity $|\mathbf{v}_0|$ to go through a substantial amount of collisions so as to begin significant thermalization. Such a scenario may be orchestrated by the creation of a plasma state with a high-power laser pulse, where subsequently a small fraction is subjected to an ultrafast external acceleration/deceleration mechanism, which is finally irradiated by a second high-power laser pulse. The second laser pulse must also be ultrafast on the grounds that it must provide the benefit of fusion enhancement before the plasma has had a chance to thermalize again to a new temperature. For the conventional Maxwellian distribution, the peak and average energy are given by $k_BT/2$ and $3k_BT/2$, respectively, which for our considered $T = 3$ keV yields 1.5 keV and 4.5 keV. We consider a set of values for the parameter $\mathcal{E}_0$ that contain values smaller and larger than both the peak and average energy of the original Maxwellian. The resulting distributions are shown in Fig. 5.

The main features we wish to highlight from Fig. 5 are the following: a disembarkation from the fully Maxwellian distribution leads to (i) a reduction in the peak value of $f(\mathcal{E}, \mathcal{E}_0)$, (ii) a slight shift of the peak value to higher values of $\mathcal{E}$, and (iii) a widening of the resulting distribution, for all considered values of $\mathcal{E}_0$. So, how can this behavior aid us in the resulting

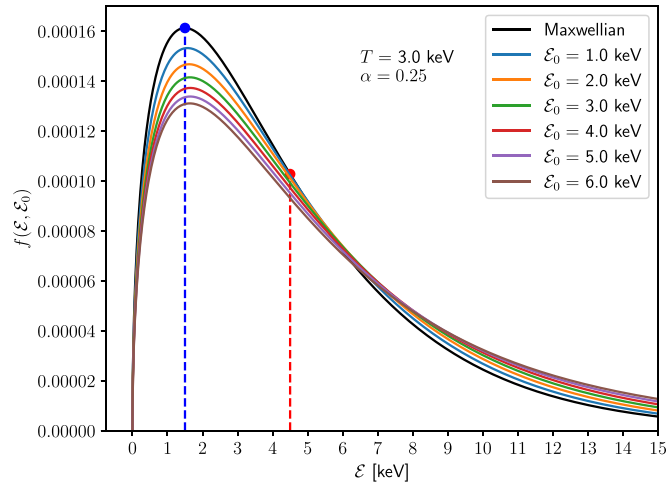

FIG. 5. The energy distribution $f(\mathcal{E}, \mathcal{E}_0)$ from Eq. (29) as a function of the CoM energy $\mathcal{E}$, at $\alpha = 0.25$, with $\mathcal{E}_0$ ranging from 1.0–6.0 keV. These values were chosen such that the peak and average energy of the original Maxwellian distribution lie within this range. For the considered temperature of $T = 3$ keV, these values are 1.5 keV (blue dotted line) and 4.5 keV (red dotted line), respectively. The original Maxwellian distribution is shown as the black line.

reactivity? With the new distribution function, the reactivity becomes

$$\begin{aligned} \langle \sigma v \rangle &= \int d^3\mathbf{v} f(\mathbf{v}, \mathbf{v}_0) \sigma(v) v \\ &= \int d\mathcal{E} f(\mathcal{E}, \mathcal{E}_0) \sigma(\mathcal{E}) \sqrt{\frac{2\mathcal{E}}{\mu}}. \end{aligned} \tag{30}$$

The behavior of the relevant laser-enhanced cross section in the aforementioned picture can be found in our previous work [22] (in particular Fig. 7). We summarize the relevant trends: (i) for the CoM energies considered, $\sigma(\mathcal{E})$ is an increasing function, (ii) the enhancement to the cross section is larger for smaller values of $\mathcal{E}$ and becomes nearly unnoticeable for larger $\mathcal{E}$ values, and (iii) the enhanced cross section has no local minima, i.e., the enhanced cross section at a lower $\mathcal{E}$ is never greater than that at a higher $\mathcal{E}$. This allows us to justify some expected behavior. The non-Maxwellian distribution assigns smaller/larger weights to smaller/larger values of $\mathcal{E}$ as compared to the conventional Maxwellian. Since the cross section is larger at higher values of $\mathcal{E}$, we expect an increase in the reactivity. This is also true without the supposed laser enhancement. However, we expect a further increase to the reactivity in that case, so long as the enhancement to the cross section at these higher $\mathcal{E}$ values, where $f(\mathcal{E}, \mathcal{E}_0)$ exceeds the original Maxwellian, is non-negligible.

The effect of the non-Maxwellian distribution from Fig. 5 to the burn fraction is presented in Fig. 6. Considering the fact that in principle we have the fusion fuels, the number density, the temperature, the electric-field strength, the photon energy, and the energy $\mathcal{E}_0$ as free parameters, we opted for showing only a best-case scenario in Fig. 6, *vis-a-vis* laser parameters. We consider the same parameters as shown in Fig. 5, along with $n_0 = n_{\text{high}} = 7.25 \times 10^{26}$ cm^{-3}, $|\mathbf{E}| = 10^{17}$, and $\hbar\omega = 1$

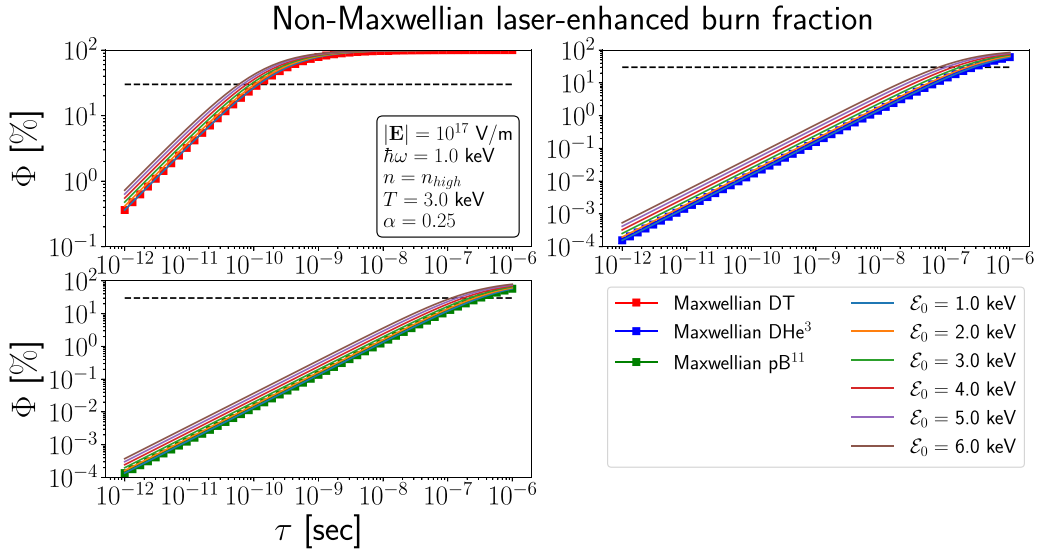

FIG. 6. The laser-enhanced burn fraction of DT (top left), DHe^3 (top right), and pB^{11} (bottom left) assuming the non-Maxwellian distribution $f(\mathcal{E}, \mathcal{E}_0)$ from Eq. (29) at the same parameters shown in Fig. 5. For the laser enhancement, only the best-case scenario was considered, i.e., $n_0 = n_{\text{high}} = 7.25 \times 10^{26}$ cm^{-3}, $|\mathbf{E}| = 10^{17}$, and $\hbar\omega = 1$ keV. Results using the conventional Maxwellian are denoted with squares and the black dotted line again denotes a burn fraction of 30%.

keV. Each of the fusion fuels DT, DHe^3, and pB^{11} are considered separately, depicted in the top left, top right and bottom left of Fig. 5, respectively. The field-free burn fraction is not shown, instead favoring to focus on the difference between the Maxwellian and non-Maxwellian results. We can see that the latter result in a further enhancement of at most a factor of ∼3–5 for all fuels, similar to the conclusion of Ref. [31]. Of course, raising α or $\mathcal{E}_0$ may increase this enhancement, but achieving this in reality poses its own technological challenges.

We can use the result from Fig. 5 and the logic in the paragraph following Eq. (30) to draw some preliminary conclusions on whether or not neglecting the effect of the laser field on the ion velocity, or energy, distribution led to an overestimate of the fusion reactivity. Of course, introducing a high-intensity laser pulse to the fusing plasma will result in a highly nonthermal ionic energy distribution, which will look nothing like the simple double Maxwellian considered earlier. However, we do expect similar behaviors, i.e., a reduction of the main peak and an increase in the tail at higher CoM energies. An increased value of the energy distribution, $f(\mathcal{E}, \mathcal{E}_0)$, will lead to enhancements to the reactivity, so long as the cross section is an increasing function of the CoM energy. This is the case before reaching the peak cross-section values at $\mathcal{E} = 64$ keV, $\mathcal{E} = 250$ keV, and $\mathcal{E} = 550$ keV, for DT, DHe^3, and pB^{11}, respectively (see Table I). However, since ions are regularly accelerated to well within the MeV range in laser-plasma experiments, this would indicate that considering a nonthermal distribution would generally reduce the fusion reactivity. Thus, neglecting the effects of the laser field on the ion distributions, as we have, led to a further overestimate of the fusion reactivities.

Finally, it is worth commenting on the seminal work by Rider [32], which essentially shows that a non-Maxwellian plasma fusion reactor is not able to produce net power. They consider decoupling the two ion species acting as fusion fuel, which are found to thermalize on a timescale much faster than the one needed to fuse. This is not so relevant for the assumption in this section. However, they also considered a non-Maxwellian, but isotropic, velocity distribution, albeit with a single peak that allowed for two temperatures related to the widths of the distribution to the left and right of the peak. Though not exactly the same, it is very similar to the scenario assumed in this section. It was found that the power needed to maintain such a distribution outweighed the potential benefits of fusion power gain in such a scenario. However, the work in Ref. [32] considers a steady-state plasma, whereas it was already alluded to in this section that the approach here occurs on an incredibly short timescale in a pulsed scenario. Moreover, we may be getting ahead of ourselves by considering potential net power of a fusion reactor, since we are assuming the introduction of a laser pulse as powerful as, and indeed more powerful than, what is currently technologically available. The purpose of this section was merely to examine to what extent the proposed non-Maxwellian distribution aids the laser-enhancement fusion further.

IV. CONCLUSIONS AND OUTLOOK

In this paper, we have examined the effects of a high-power laser on the fusion burn fraction on several fusion fuels. We used the previously validated theoretical framework of the Floquet-Volkoff (FV) method to characterize these laser-induced enhancements and obtain subsequent reactivity estimates. We note that the subsequently calculated burn fractions are upper estimates considering the fact that we did not take volume expansion into account. That notwithstanding, we did account for fuel depletion, varying fuel mixtures, and an arbitrary method of confining the fuel to induce fusion.

We first considered some idealized plasma states of each fuel for conditions that resulted in an appreciable burn. Within our framework, we found that the best fuel mixture was an equimolar one. We argued that if the effect of laser enhancement to the fusion reactivity is to be useful, an upper limit is set on the plasma density, requiring unrealistically high values for the temperature if the peak of the reactivity is meant to be reached.

Subsequently, we considered more realistic laser-and-plasma parameters and calculated the laser-enhanced burn fraction with the FV method. We found that the largest relative enhancement to the burn fraction was found for those fuel partners with the highest relative charge numbers, similar to the trend reported in Ref. [22]. Therefore, the DT burn fraction had the least to gain from the laser enhancement, but still had the highest burn fraction among all considered fusion fuels for all parameters considered. Appreciable burn of DT could be achieved on a subnanosecond confinement timescale at the most extreme conditions considered ($n_0 = 7.25 \times 10^{26}$ cm^{-3}, $|\mathbf{E}| = 10^{17}$, and $\hbar\omega = 1$ keV).

At these same parameters, we found that the burn fractions of DHe^3 and pB^{11} could be enhanced by many orders of magnitude, but even then, appreciable burn did not occur for confinement times below ∼50 ns. However, due to the aforementioned effect of the charge numbers on the relative enhancement, the enhanced pB^{11} burn fraction was nearly able to surpass the enhanced DHe^3 burn fraction, at these parameters.

Finally, we considered if a non-Maxwellian velocity distribution could potentially aid the laser-induced enhancement further. We found that, indeed, further enhancement could be obtained, but it remained within an order of magnitude for the most extreme laser parameters mentioned before. In addition, obtaining such a distribution is by no means trivial and it is uncertain whether it is realizable.

Thus, we conclude that for current technologically available high-power lasers, the laser-induced enhancement leaves the DT burn fraction largely unaffected and, though they may enhance the burn fractions of the other fuels, it fails to enhance these enough to obtain similar appreciable burn fractions. Nevertheless, these results were obtained in what is essentially an effective two-body framework. No loss mechanisms, such as bremsstrahlung, volumetric expansion, and heat transfer from electron conduction, were considered as they bear no relevance in comparing burn fraction with and without the effects of an intense laser field. Also, the entire plethora of plasma and environment effects were not accounted for. This includes electron screening and, similar to how a plasma environment causes ionization potential depression [33] making it easier to ionize ions further, it is expected that similarly fusion is made easier under these conditions. Furthermore, ion ranges are typically larger in a plasma state as compared to a cold solid, which can further increase fusion reactions [34]. However, considering the many orders of magnitude in enhancement these effects would have to overcome, we would cautiously conclude that laser-induced enhancement to fusion is not a technologically viable option at this time, at least not on its own. It may find applications in a regime marginal to igniting nuclear burn waves.

ACKNOWLEDGMENTS

We acknowledge funding by Marvel Fusion GmbH. This work is in part supported by the U.S. Department of Energy (DOE), Office of Science, Fusion Energy Sciences, FWP No. 0024882: IFE-STAR. Considering the conclusion of this work, this avenue of research is no longer under active investigation by Marvel Fusion GmbH. For up-to-date information on the Marvel Fusion concept, see Refs. [35–38].

[1] D. D. Clayton, *Principles of Stellar Evolution and Nucleosynthesis*, 2nd ed. (The University of Chicago Press, Chicago, 1983).

[2] W. C. Elmore, E. M. Little, and W. E. Quinn, Neutrons of possible thermonuclear origin, Phys. Rev. Lett. **1**, 32 (1958).

[3] V. P. Smirnov, Tokamak foundation in USSR/Russia 1950-1990, Nucl. Fusion **50**, 014003 (2010).

[4] J. H. Nuckolls, Early steps toward inertial fusion energy (IFE) (1952 to 1962), United States: N. p., 1998, doi:10.2172/658936.

[5] G. L. Kulcinski, M. E. Sawan, and I. N. Sviatoslavsky, Nuclear design and analysis of ITER: Progress report, November 15, 1987–November 14, 1988, Technical Report No. DOE/ER/52140-2; ON: DE89003816 (OSTI, USA, 1988), https://www.osti.gov/biblio/6689059.

[6] P. Rodriguez-Fernandez, A. J. Creely, M. J. Greenwald, D. Brunner, S. B. Ballinger, C. P. Chrobak, D. T. Garnier, R. Granetz, Z. S. Hartwig, N. T. Howard *et al.*, Overview of the SPARC physics basis towards the exploration of burning-plasma regimes in high-field, compact tokamaks, Nucl. Fusion **62**, 042003 (2022).

[7] A. B. Zylstra, O. A. Hurricane, D. A. Callahan, A. L. Kritcher, J. E. Ralph, H. F. Robey, J. S. Ross, C. V. Young, K. L. Baker, D. T. Casey *et al.*, Burning plasma achieved in inertial fusion, Nature (London) **601**, 542 (2022).

[8] A. L. Kritcher, C. V. Young, H. F. Robey, C. R. Weber, A. B. Zylstra, O. A. Hurricane, D. A. Callahan, J. E. Ralph, J. S. Ross, K. L. Baker *et al.*, Design of inertial fusion implosions reaching the burning plasma regime, Nat. Phys. **18**, 251 (2022).

[9] H. Abu-Shawareb, R. Acree, P. Adams, J. Adams, B. Addis, R. Aden, P. Adrian, B. B. Afeyan, M. Aggleton, L. Aghaian *et al.*, Lawson criterion for ignition exceeded in an inertial fusion experiment, Phys. Rev. Lett. **129**, 075001 (2022).

[10] A. L. Kritcher, A. B. Zylstra, D. A. Callahan, O. A. Hurricane, C. R. Weber, D. S. Clark, C. V. Young, J. E. Ralph, D. T. Casey, A. Pak *et al.*, Design of an inertial fusion experiment exceeding the Lawson criterion for ignition, Phys. Rev. E **106**, 025201 (2022).

[11] A. B. Zylstra, A. L. Kritcher, O. A. Hurricane, D. A. Callahan, J. E. Ralph, D. T. Casey, A. Pak, O. L. Landen, B. Bachmann, K. L. Baker *et al.*, Experimental achievement and signatures of ignition at the National Ignition Facility, Phys. Rev. E **106**, 025202 (2022).

[12] J. Tollefson, Exclusive: Laser-fusion facility heads back to the drawing board, Nature (London) **608**, 20 (2022).

[13] F. Queisser and R. Schützhold, Dynamically assisted nuclear fusion, Phys. Rev. C **100**, 041601(R) (2019).
[14] S. Liu, H. Duan, D. Ye, and J. Liu, Deuterium-tritium fusion process in strong laser fields: Semiclassical simulation, Phys. Rev. C **104**, 044614 (2021).
[15] J. J. Bekx, M. L. Lindsey, S. H. Glenzer, and K.-G. Schlesinger, Applicability of semiclassical methods for modeling laser-enhanced fusion rates in a realistic setting, Phys. Rev. C **105**, 054001 (2022).
[16] W. Lv, H. Duan, and J. Liu, Enhanced deuterium-tritium fusion cross sections in the presence of strong electromagnetic fields, Phys. Rev. C **100**, 064610 (2019).
[17] C. Kohlfürst, F. Queisser, and R. Schützhold, Dynamically assisted tunneling in the impulse regime, Phys. Rev. Res. **3**, 033153 (2021).
[18] W. Lv, B. Wu, H. Duan, S. Liu, and J. Liu, Phase-dependent cross sections of deuteron-triton fusion in dichromatic intense fields with high-frequency limit, Eur. Phys. J. A **58**, 54 (2022).
[19] W. Lv, H. Duan, and J. Liu, Enhanced proton-boron nuclear fusion cross sections in intense high-frequency laser, Nucl. Phys. A **1025**, 122490 (2022).
[20] B. Wu, H. Duan, and J. Liu, Resonant tunneling of deuteron-triton fusion in strong high-frequency electromagnetic fields, Phys. Rev. C **105**, 064615 (2022).
[21] X. Wang, Substantially enhanced deuteron-triton fusion probabilities in intense low-frequency laser fields, Phys. Rev. C **102**, 011601(R) (2020).
[22] J. J. Bekx, M. L. Lindsey, and K.-G. Schlesinger, Effect of nuclear charge on laser-induced fusion enhancement in advanced fusion fuels, Phys. Rev. C **106**, 034003 (2022).
[23] M. L. Lindsey, J. J. Bekx, K.-G. Schlesinger, and S. H. Glenzer, Dynamically assisted nuclear fusion in the strong-field regime, Phys. Rev. C **109**, 044605 (2024).
[24] D. Ryndyk, C. Kohlfürst, F. Queisser, and R. Schützhold, Dynamically assisted tunneling in the Floquet picture, Phys. Rev. Res. **6**, 023056 (2024).
[25] S. Atzeni and J. Meyer-ter-Vehn, *The Physics of Inertial Fusion: Beam Plasma Interaction, Hydrodynamics, Hot Dense Matter* (Oxford University Press, Oxford, 2004).
[26] H.-S. Bosch and G. M. Hale, Improved formulas for fusion cross-sections and thermal reactivities, Nucl. Fusion **32**, 611 (1992).
[27] W. M. Nevins and R. Swain, The thermonuclear fusion rate coefficient for p-^{11}B reactions, Nucl. Fusion **40**, 865 (2000).
[28] Though it is more common to use the areal density, ρR, in ICF, with ρ the average mass density of the fusing plasma and R its radius, this fixes the volumetric geometry, as evidenced by the presence of R. For this reason, we stuck to the product $n\tau$, used more conventionally in magnetic confinement fusion.
[29] J. D. Lawson, Some criteria for a power producing thermonuclear reactor, Proc. Phys. Soc. B **70**, 6 (1957).
[30] R. Majumdar and D. Das, Estimation of total fusion reactivity and contribution from supra-thermal tail using 3-parameter Dagum ion speed distribution, Ann. Nucl. Energy **97**, 66 (2016).
[31] S. V. Putvinski, D. D. Ryutov, and P. N. Yushmanov, Fusion reactivity of the pB^{11} plasma revisited, Nucl. Fusion **59**, 076018 (2019).
[32] T. H. Rider, Fundamental limitations on plasma fusion systems not in thermodynamic equilibrium, Phys. Plasmas **4**, 1039 (1997).
[33] J. J. Bekx, S.-K. Son, B. Ziaja, and R. Santra, Electronic-structure calculations for nonisothermal warm dense matter, Phys. Rev. Res. **2**, 033061 (2020).
[34] Y. Zhang, Z. Zhang, B. Zhu, W. Jiang, X. Zhang, X. Zhao, X. Yuan, J. Zhong, S. He, F. Lu *et al.*, Ion beam stopping power effects on nuclear fusion reactions, Phys. Plasmas **29**, 103103 (2022).
[35] H. Ruhl and G. Korn, A laser-driven mixed fuel nuclear fusion micro-reactor concept, arXiv:2202.03170.
[36] H. Ruhl and G. Korn, High current ionic flows via ultra-fast lasers for fusion applications, arXiv:2212.12941.
[37] H. Ruhl and G. Korn, Uniform volume heating of mixed fuels within the ICF paradigm, arXiv:2302.06562.
[38] H. Ruhl and G. Korn, Numerical validation of a volume heated mixed fuel concept, arXiv:2306.03731.